

MI-ISAC: Magneto-Inductive Integrated Sensing and Communication in the Reactive Near-Field for RF-Denied Environments

Haofan Dong, *Student Member, IEEE*, and Ozgur B. Akan, *Fellow, IEEE*

Abstract—Radio-frequency integrated sensing and communication (RF-ISAC) is ineffective in underground, underwater, and in-body environments where conductive media attenuate electromagnetic waves by tens of dB per meter. This article presents magneto-inductive ISAC (MI-ISAC), a paradigm that exploits the reactive near-field quasi-static coupling inherent to MI links, enabling a fundamentally different approach to ISAC in these RF-denied environments. Five foundational results are established: (i) tri-axial coils are necessary and sufficient for identifiable joint range-and-angle estimation; (ii) coupling strength changes sharply with range, enabling theoretical sub-millimeter accuracy at typical MI distances despite kHz-level bandwidth; (iii) time-of-flight is ineffective under such narrow bandwidth, but the coupling gradient provides approximately six orders of magnitude finer resolution; (iv) MI-ISAC can provide 4–10+ dB sensing gain over time-division baselines; and (v) the MI-MIMO channel is geometry-invariant and well-conditioned across all orientations. Applications and a research roadmap are discussed.

Index Terms—Magnetic induction, integrated sensing and communication, reactive near-field, tri-axial coils, Cramér–Rao bound, RF-denied environments, underground communication, MIMO coupling tensor.

I. INTRODUCTION

THE vision of 6G wireless systems places integrated sensing and communication (ISAC) at center stage: a single platform simultaneously transmits data and perceives its physical environment [1], [2]. Yet the existing ISAC literature is built upon radio-frequency (RF) electromagnetic wave propagation—a premise that does not hold in three domains.

Underground. Soil and rock absorb RF energy at 10–30 dB/m (sub-GHz), restricting conventional radar and communication to a few meters. Mining rescue, pipeline integrity monitoring, precision agriculture, and seismic early-warning networks all require coexisting communication and localization capabilities that RF-ISAC cannot provide [3], [4]. In these scenarios, knowing *where* an underground sensor sits is as important as the data it reports.

Underwater. Seawater conductivity (≈ 4 S/m) limits RF to centimeters; acoustic links impose ~ 1 s/km latency, hindering real-time AUV control [5].

In-body. Biological tissue absorbs RF significantly, and SAR limits constrain power to milliwatts. Next-generation implants need bidirectional telemetry coupled with local tissue sensing for closed-loop therapy [6].

H. Dong and O. B. Akan are with the Internet of Everything Group, Department of Engineering, University of Cambridge, Cambridge CB3 0FA, U.K. (e-mail: hd489@cam.ac.uk; oba21@cam.ac.uk).

Ozgur B. Akan is also with the Center for neXt-generation Communications (CXC), Department of Electrical and Electronics Engineering, Koç University, 34450 Istanbul, Turkey (email: oba21@cam.ac.uk).

All three domains require co-located communication and sensing—the ISAC mandate—which RF-ISAC cannot adequately address (Fig. 1).

Recent near-field ISAC work uses large arrays in the *radiative* Fresnel region [7], where sensing still relies on ToF/Doppler with a spherical-wave refinement. MI operates in the *reactive* near field, where radiation is negligible and interaction is dominated by quasi-static magnetic coupling—so the physics, models, and design tools require substantial revision.

This article introduces MI-ISAC as a new paradigm and presents five quantifiable results:

- 1) **MI-ISAC framework**: MI-ISAC is defined formally and it is shown that, to the best of our knowledge, no prior work exists at the MI×ISAC intersection, despite the IEEE COMST 2025 MI survey [6] noting this as an open area.
- 2) **Resolution paradigm shift**: MI-ISAC ranging resolution is determined by the coupling gradient (r^{-3} amplitude), not bandwidth; the RF ToF limit is inapplicable at MI bandwidths ($c/2B = 150$ km at 1 kHz).
- 3) **Identifiability and CRB**: Tri-axial coils yield a full-rank Fisher information matrix (FIM) for (r, θ, ϕ) ; single-axis coils are rank-deficient. The CRB scales as r^8 in closed form.
- 4) **MI-MIMO structure**: The dipole coupling tensor G has eigenvalues $\{+2, -1, -1\}$, giving rank = 3 and $\kappa = 2$ universally.
- 5) **Quantifiable ISAC gain**: MI-ISAC can achieve 4–10+ dB sensing gain over a TDMA baseline, decomposed into a 3-dB time-multiplexing term and a 1–9 dB structural-information term.

II. MI COMMUNICATION FUNDAMENTALS

A. From Wave Propagation to Quasi-Static Coupling

In conventional RF communication, information is carried by electromagnetic waves that radiate from a transmitter and propagate through space at the speed of light. In MI communication, information transfer occurs through a different mechanism: *reactive near-field magnetic coupling* [8]. A transmitter coil generates a quasi-static magnetic field; a receiver coil experiences induced voltage proportional to mutual inductance. Propagation delay is negligible—energy exchanges through flux linkage rather than radiation.

The implication for sensing: with negligible propagation delay, the received signal strength depends solely on geometry and the medium—precisely the basis of MI-ISAC sensing. Moreover, since $\mu \approx \mu_0$ in soil, seawater, and tissue, MI path loss is largely medium-independent, unlike RF [8], [9].

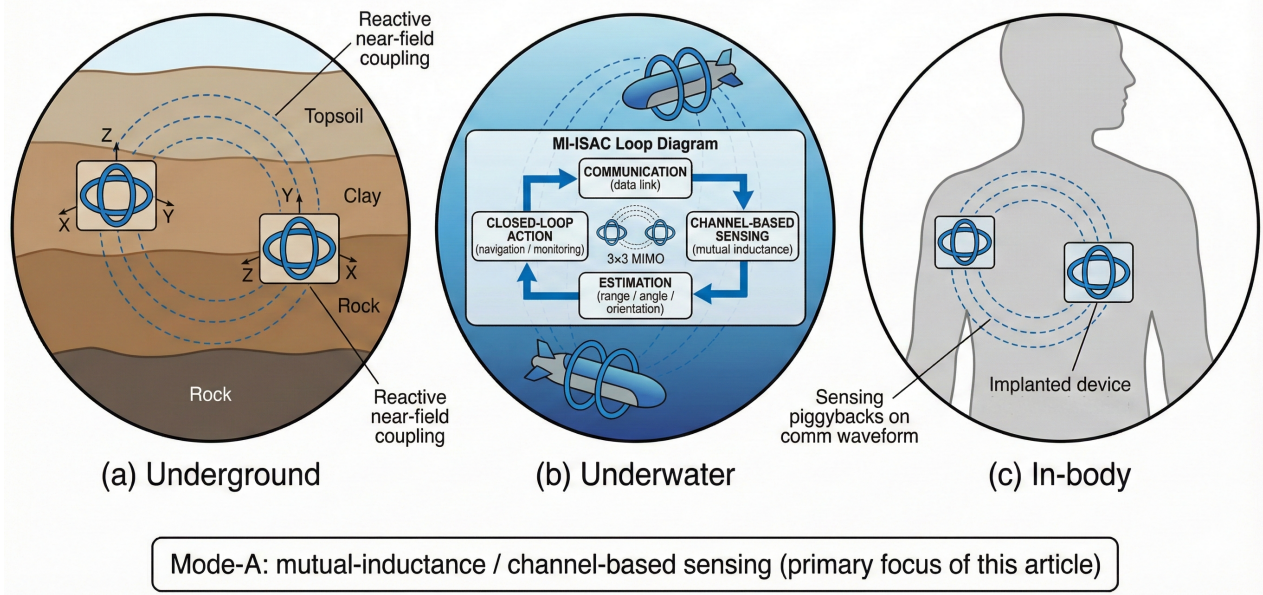


Fig. 1. MI-ISAC concept: three RF-denied environments (underground, underwater, in-body) unified by a single reactive near-field coupling link. The central MI-ISAC loop illustrates how communication, channel-based sensing, parameter estimation, and closed-loop control share the same waveform and hardware through the geometry-deterministic 3×3 MI-MIMO channel.

B. The Deterministic MI Channel

Consider a Tx and Rx coil separated by distance r , each with N_t turns and radius a , operating at angular frequency $\omega_0 = 2\pi f_0$ (Fig. 2). In the magnetic dipole approximation ($a \ll r \ll \lambda$), the channel coefficient is:

$$h(r, \theta, \phi) = \frac{C}{r^3} \cdot g(\theta, \phi), \quad (1)$$

with C a known coil-dependent constant¹ and $g(\theta, \phi)$ encoding the orientation dependence through the dipole coupling tensor G . The received signal is the transmitted symbol scaled by the channel coefficient plus additive white Gaussian noise.

Two properties of (1) are central to MI-ISAC. First, the channel is *deterministic*: it exhibits negligible fading, multipath, and stochastic variation—a known, invertible function of geometry. Second, it has a *pronounced gradient*: the r^{-3} amplitude dependence creates a sensitivity that scales as r^{-4} —a limitation for communication range but a significant advantage for range estimation.

C. Tri-Axial Coils and 3×3 MIMO

A single-axis coil captures only the projection of the magnetic field along its normal. To recover the full vector field, each node is equipped with *three mutually orthogonal coils*—a tri-axial configuration—creating a 3×3 MI-MIMO channel whose entries are governed by the dipole coupling tensor G (Fig. 2). Tri-axial coil hardware is well-established: it has been demonstrated in underground MI networks [10], magneto-inductive positioning systems [11], and medical telemetry [6]. As shown in Section IV, the tri-axial architecture is not only beneficial but *necessary* for identifiable sensing: single-axis coils cannot uniquely determine all three spatial parameters.

¹ $C = \mu_0 \omega_0 N_t^2 A^2 / (4\pi)$ with $A = \pi a^2$ the coil area; in practice C is calibrated per deployment to absorb coil non-idealities.

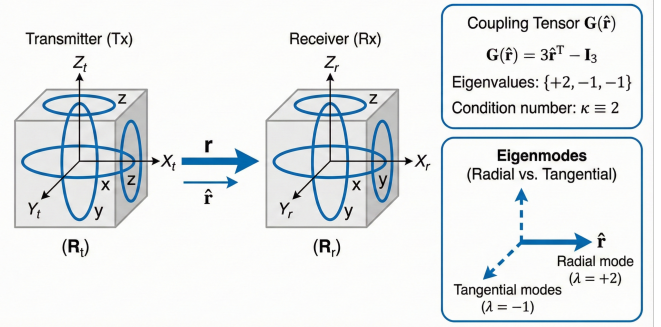


Fig. 2. MI channel model and tri-axial coil geometry. Two nodes with local coordinate frames (X_t, Y_t, Z_t) and (X_r, Y_r, Z_r) are separated by vector r . The coupling tensor $G = 3\hat{r}\hat{r}^T - I_3$ has eigenvalues $\{+2, -1, -1\}$ and corresponding radial/tangential eigenmodes.

III. MI-ISAC: CONCEPT AND SYSTEM ARCHITECTURE

A. What Is MI-ISAC?

MI-ISAC is defined as follows: *a system in which the same set of MI communication symbols and packet structure simultaneously supports both data transmission and estimation of physical parameters (r, θ, ϕ) or environmental parameters (σ_m), using a single hardware platform without dedicated sensing waveforms or additional spectral resources.*

This definition distinguishes MI-ISAC from prior work on MI-based localization [4], [11], [12], which treated positioning and communication as separate functions using distinct time slots or frequency bands. The most relevant prior work, Lin *et al.* [12], performed sequential MI communication then MI localization—a partially integrated design analogous to time-division ISAC. The framework presented here targets *full integration* at the waveform level.

Table I contrasts RF-ISAC, MI-ISAC, and the prior MI positioning-plus-communication approach across seven dimensions, making the fundamental distinctions explicit.

B. Sensing Modes: Mode A vs. Mode B

MI-ISAC sensing can operate in two complementary modes. **Mode A (Bistatic, Link-Mediated)** extracts parameters from the mutual-inductance channel $h(r, \theta, \phi, \sigma_m)$ between Tx and Rx. Each communication symbol carries sensing information through its amplitude and phase. This is the primary mode addressed in this article—it enables low-overhead sensing because the receiver already estimates the channel for demodulation; inverting the deterministic channel model to obtain geometric parameters requires only additional computation, no additional signaling. **Mode B (Monostatic, Self-Impedance)** detects nearby conductors via eddy-current-induced impedance changes [13], but exhibits r^{-6} decay limiting range to 5–10 m; it is treated as a future extension.

C. MI-ISAC Transceiver Architecture

A minimal MI-ISAC transceiver generates standard communication frames: a short preamble for synchronization followed by data symbols. The Rx performs three parallel tasks: synchronization and frequency tracking; channel estimation followed by data demodulation (communication path); and parameter extraction from the estimated channel (sensing path). In the sensing path, the main operation is *channel inversion*: the receiver extracts range from the estimated channel magnitude and angles from the eigenstructure of the estimated coupling tensor. Because \mathbf{H} is a deterministic, bijective function of (r, θ, ϕ) , this inversion is well-posed whenever the FIM is full-rank—a condition guaranteed by the tri-axial architecture. Since channel estimation is already performed for coherent demodulation, the only added sensing cost is a lightweight algebraic inversion—achieving sensing at negligible additional overhead.

IV. KEY RESULTS: FIVE FOUNDATIONAL INSIGHTS

A. Insight 1: Tri-Axial Is Necessary for Identifiability

The fundamental question for any sensing system is: *can the parameters of interest be uniquely determined from observations?* For MI-ISAC, the goal is to estimate range, azimuth, and elevation from received signals. The Fisher information matrix (FIM) captures the available information; identifiability requires the FIM to be full-rank.

Under narrowband MI mutual-inductance observations, a single-axis coil yields a rank-deficient FIM, making joint estimation of (r, θ, ϕ) infeasible. The intuition is straightforward: a single scalar observation $|h|$ couples r , θ , and ϕ through one equation—three unknowns from a single equation, hence rank deficiency. A tri-axial coil configuration at both Tx and Rx, however, yields a full-rank FIM for all non-degenerate geometries, because the 3×3 matrix observation \mathbf{H} provides up to 9 independent real measurements (6 unique due to symmetry), more than sufficient to resolve 3 parameters. Fig. 3(a) illustrates this via the FIM rank comparison. This implies that

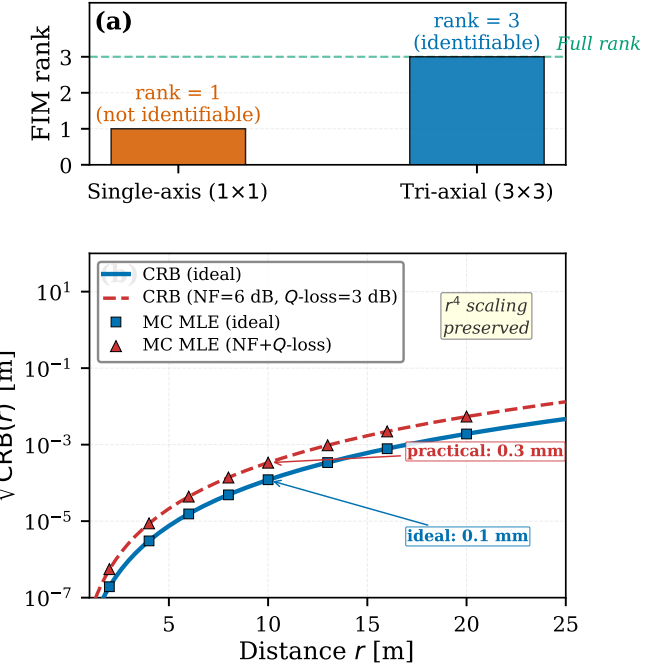


Fig. 3. (a) FIM rank: single-axis (rank = 1, not identifiable) vs. tri-axial (rank = 3, identifiable). (b) $\sqrt{\text{CRB}(r)}$ vs. distance showing r^4 scaling (equivalently r^8 in CRB). Blue: ideal thermal noise; red: practical front-end (NF = 6 dB, finite- Q loss = 3 dB). MC MLE markers validate both bounds. At $r = 10$ m: 0.1 mm (ideal) vs. 0.3 mm (practical)—both sub-millimeter. Parameters: $a = 0.15$ m, $N_t = 20$, $f_0 = 10$ kHz, $N = 100$, $P = 1$ W, $B = 1$ kHz.

tri-axial coils are not only beneficial but necessary for MI-ISAC. While the dipole tensor eigenstructure is established in electromagnetics, its role as an *identifiability enabler* for joint communication-and-sensing is, to our knowledge, new.

B. Insight 2: CRB Scales as r^8

Given identifiability, the next question is: *how precisely can r be estimated?* Because the channel amplitude decays as r^{-3} , its gradient with respect to range scales as r^{-4} . Squaring this gradient in the Fisher information yields the Cramér–Rao bound:

$$\text{CRB}(r) = \frac{\sigma_w^2 r^8}{18 N P |C|^2}, \quad (2)$$

where N is the number of observed symbols, P the transmit power, and σ_w^2 the noise variance.

The r^8 scaling arises from the r^{-3} coupling law. While this implies rapid degradation at long range, at typical MI communication distances (1–30 m) it enables high precision in principle. For representative underground parameters ($a = 0.15$ m, $N_t = 20$, $f_0 = 10$ kHz, $N = 100$, $P = 1$ W), the root-CRB, representing the theoretical lower bound, at 10 m is approximately 0.1 mm under ideal thermal noise—a theoretical limit of sub-millimeter ranging accuracy from a narrowband 10 kHz link. Fig. 3(b) validates the r^8 scaling via Monte Carlo MLE that achieves the bound under both ideal and practical front-end conditions (noise figure 6 dB, finite- Q insertion loss 3 dB); the latter shifts the CRB upward by 9 dB but preserves the r^8 law, with both curves remaining sub-millimeter at 10 m.

TABLE I
FUNDAMENTAL COMPARISON: RF-ISAC VS. MI-ISAC (MODE A) VS. PRIOR MI POSITIONING-PLUS-COMMUNICATION

Attribute	RF-ISAC	MI-ISAC (this work)	Prior MI pos.+comm.
EM regime	Radiative far/near-field	Reactive near-field	Reactive near-field
Sensing mechanism	ToF / Doppler	Coupling strength & tensor	RSS fingerprinting
Channel model	Stochastic (fading)	Deterministic $h(r, \theta, \phi)$	Deterministic
Integration level	Waveform-level	Waveform-level	Time-division (partial)
MIMO structure	Array manifold; κ depends on scattering	Dipole tensor G , $\kappa \equiv 2$	Single-axis typical
Resolution source	Bandwidth B	Coupling gradient r^{-3}	Calibration database
Target environment	LoS air / indoor	RF-denied media	RF-denied media

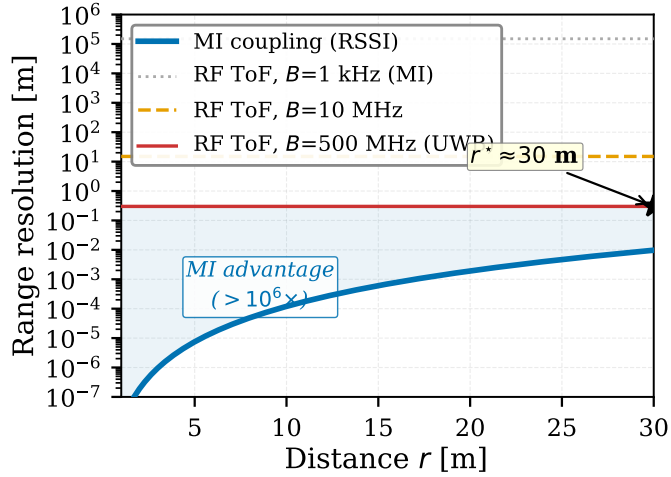


Fig. 4. Resolution comparison: MI coupling-based (RSSI) vs. RF ToF at various bandwidths. Within the MI communication range ($r < r^*$), MI achieves over three orders of magnitude finer resolution than 500 MHz UWB. The paradigm shift: from bandwidth-limited ToF to gradient-limited RSSI.

C. Insight 3: ToF Provides Limited Resolution; Coupling Gradient Dominates

RF-ISAC extracts range from the round-trip propagation delay, yielding a resolution limit of $c/(2B)$. At MI bandwidth $B = 1\text{ kHz}$, this gives 150 km—approximately six orders of magnitude coarser than the sub-millimeter MI coupling-based resolution, rendering ToF-based ranging *unsuitable* at MI bandwidths.

MI-ISAC instead exploits the pronounced r^{-3} amplitude dependence, which creates a measurable signal change for sub-millimeter displacements. This is *gradient-based ranging* rather than *delay-based ranging*. The crossover distance r^* below which MI outperforms even wideband RF (500 MHz UWB, resolution 0.3 m) is on the order of 10 m for representative parameters, comfortably within the typical MI communication range. Fig. 4 illustrates this paradigm shift: within the MI operating region, MI achieves over three orders of magnitude finer resolution than UWB.

D. Insight 4: 4–10+ dB ISAC Gain over TDMA

To quantify the benefit of *integrating* sensing with communication rather than separating them in time, MI-ISAC is compared against a TDMA baseline where a fraction α of the frame is allocated to dedicated sensing pilots. MI-ISAC uses the *entire N-symbol frame* for both functions, while TDMA

uses only αN symbols for sensing. The CRB ratio yields a sensing gain inversely proportional to the pilot fraction α (in dB), which decomposes into two interpretable terms.

The first is a *time-multiplexing gain*: at $\alpha = 0.5$ (half the frame for sensing), MI-ISAC observes twice as many sensing symbols, yielding a 3 dB advantage. The second is a *structural-information gain* of 1–9 dB: the deterministic MI channel enables non-data-aided (NDA) estimation from *each* received symbol—including data symbols—without additional overhead. In TDMA, only dedicated pilots contribute to sensing. At sufficiently high MI-range SNR (tens of dB, typical in the short-range reactive near field), NDA channel estimation approaches data-aided performance because the constellation-removal penalty becomes negligible: each symbol can serve as a sensing pilot. The structural gain increases with SNR and the number of coil axes, reaching 6–9 dB for tri-axial configurations. For practical sensing allocations ($\alpha = 0.1$ –0.5), the total gain is 3–10+ dB.

E. Insight 5: MI-MIMO—rank=3 and $\kappa \equiv 2$

The tri-axial MI-MIMO channel inherits the eigenstructure of the dipole coupling tensor G . A direct eigenanalysis yields eigenvalues $\{+2, -1, -1\}$ for all orientations, giving rank=3 and a universal condition number $\kappa \equiv 2$.

The eigenvector for $\lambda = +2$ is \hat{r} itself (the *radial mode*), representing the strongest coupling along the Tx–Rx axis with 4× effective power gain. The two degenerate eigenvectors ($\lambda = -1$) span the perpendicular plane (*tangential modes*), coupling to angular displacements. This eigenstructure induces a natural ISAC mode decomposition: allocate power on the radial mode for maximum communication rate, and use the tangential modes for independent angular sensing. Because eigenvalues are known *a priori* (they depend only on direction, not on fading), channel state information feedback is not required—a distinct advantage over RF-MIMO ISAC, where the condition number depends on scattering and can be arbitrarily large in line-of-sight channels. The eigenstructure itself is an established property of the magnetic dipole tensor; the contribution here is identifying its role as a *geometry-independent ISAC mode decomposer* that decouples range estimation from angular sensing.

V. USE CASES AND DEPLOYMENT SKETCHES

The three RF-denied scenarios from Fig. 1 are revisited, mapping MI-ISAC capabilities to concrete operational needs.

A. Underground: IoUT, Mining, and Pipeline Monitoring

Underground wireless sensor networks deployed for pipeline integrity monitoring, precision agriculture, and mine safety currently use MI nodes operating at 1–100 kHz with typical ranges of 5–30 m [8], [10]. MI-ISAC can augment these nodes with simultaneous ranging (inter-node distance estimation for cooperative localization), soil conductivity monitoring (σ_m from the complex channel coefficient), and link quality tracking—without additional hardware or spectral resources. The r^8 CRB scaling predicts sub-millimeter inter-node ranging at 10 m in principle, which could complement dedicated ultrasonic displacement sensors currently used for structural health monitoring. Temporal monitoring of σ_m changes could, if validated, provide early warning of water pipe leaks or ground saturation preceding landslides. Relay waveguides [14] could simultaneously serve as communication relays and distributed sensing anchors, transforming MI infrastructure into an underground sensing network.

B. Underwater: AUV Swarm Coordination

AUV swarms performing coordinated ocean-floor mapping or search-and-rescue operations require simultaneous communication and relative positioning. Acoustic ISAC is fundamentally limited by the low propagation speed of sound (1.5 km/s vs. 3×10^8 m/s), creating a latency–resolution tradeoff: centimeter-level acoustic ranging requires >10 ms round-trip times at 10 m, introducing excessive delays in real-time formation control loops [5], [15]. MI-ISAC provides a low-latency alternative with coupling-based sensing, where propagation delay is negligible at MI ranges. The $\kappa \equiv 2$ property guarantees well-conditioned positioning regardless of AUV orientation—important for maneuvering platforms where attitude changes continuously. Furthermore, the complex MI channel coefficient carries medium information: the imaginary part of the received coupling depends on seawater conductivity, potentially enabling real-time salinity and temperature mapping as an additional capability of inter-vehicle communication [9].

C. In-Body: Implantable Bioelectronic Devices

Next-generation bioelectronic implants (pacemakers, neural stimulators, closed-loop drug delivery) require both telemetry to external controllers and local tissue sensing for diagnostic feedback. MI-ISAC can enable an inductively coupled link to simultaneously carry diagnostic data and estimate tissue impedance changes indicative of edema, infection, or electrode migration [6]. This extends the biomedical “theranostics” concept (therapy + diagnostics) to the communication layer, where the telemetry link itself can serve as a diagnostic sensor. Short communication distances (<30 cm) and high coupling at low frequency make the r^8 CRB particularly suitable, potentially enabling micrometer-level resolution for implant micromotion detection.

VI. OPEN CHALLENGES AND RESEARCH ROADMAP

The open research landscape is organized into four challenge areas spanning physics, signal processing, and networking, and summarized in the roadmap of Fig. 5.

1) Model Validity and Hardware Non-Idealities. The results in this article rely on the magnetic dipole approximation ($a \ll r$), ideal coil alignment knowledge, and thermal-noise-limited reception. Practical MI transceivers face coil impedance drift with temperature, finite Q-factor limiting bandwidth, power amplifier nonlinearity, and ADC quantization noise. Fig. 3(b) provides a first-order assessment: a combined 9 dB front-end penalty shifts the CRB upward but preserves the r^8 scaling law. A systematic investigation of these impairments on the $\kappa=2$ invariant, and self-calibration protocols exploiting tri-axial redundancy (9 measurements for 3 unknowns), are potential near-term directions.

2) Multi-Node Interference and Scheduling. In networks of K MI-ISAC nodes, co-frequency mutual coupling creates inter-link interference degrading both functions. MI interference decays with the same r^{-3} order as the desired coupling; hence the signal-to-interference ratio does not improve with distance, and interference must be explicitly managed through scheduling or spatial separation.

3) ISAC Waveform and CRB–Rate Tradeoff. The RF-ISAC literature on CRB–rate region characterization and dual-function waveform design [2] provides an established analytical toolkit, but the underlying physics need to be adapted for MI. The MI-ISAC Pareto boundary between communication rate and sensing Fisher information admits a closed-form expression because the channel is deterministic, enabling globally optimal CRB–rate tradeoff designs that are intractable in stochastic RF channels. Mode decomposition (radial for communication, tangential for sensing) provides a natural starting point for waveform co-design.

4) Cooperative Localization, Benchmarking, and Field Trials. Fusing range/angle estimates from K links enables anchor-free 3D localization, where $\kappa \equiv 2$ simplifies GDOP analysis. Fair benchmarking requires standardized baselines (TDMA-MI, pilot-only MI, RF near-field ISAC) and experimental validation in soil, seawater, and tissue phantoms.

VII. CONCLUSION

This article has introduced MI-ISAC—a reactive near-field ISAC paradigm that redefines the sensing mechanism from bandwidth-limited time-of-flight to coupling-gradient-based ranging. Three key results characterize the contribution: (i) tri-axial coils are necessary and sufficient for identifiable sensing; (ii) the CRB scales as r^8 , with a theoretical limit of sub-millimeter accuracy at typical MI distances; and (iii) the MI-MIMO coupling tensor has a universal $\kappa = 2$ and rank = 3, providing well-conditioned sensing for all geometries. MI-ISAC can achieve 4–10+ dB sensing gain over time-division baselines, making sensing essentially free in high-SNR MI links. MI-ISAC can serve as a foundational building block for 6G connectivity in challenging environments—underground, underwater, and inside the human body—opening a broad design space for future investigation.

REFERENCES

- [1] F. Liu, Y. Cui, C. Masouros, J. Xu, T. X. Han, Y. C. Eldar, and S. Buzzi, “Integrated sensing and communications: Toward dual-functional wireless networks for 6G and beyond,” *IEEE J. Sel. Areas Commun.*, vol. 40, no. 6, pp. 1728–1767, Jun. 2022.

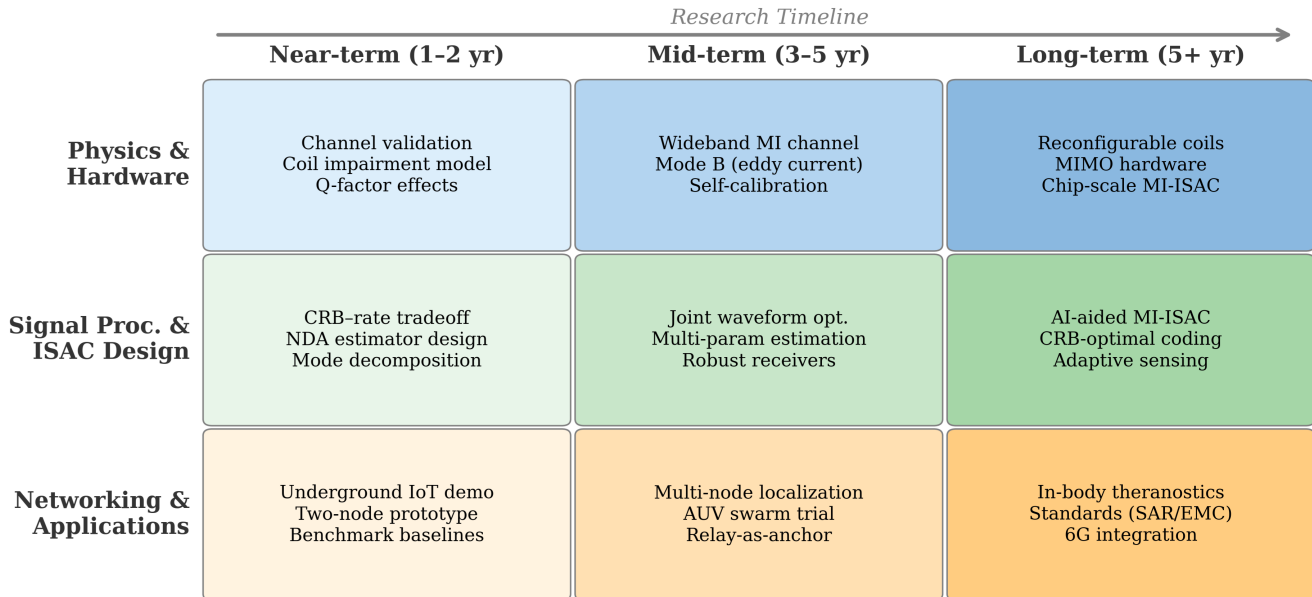


Fig. 5. MI-ISAC research roadmap: a 3x3 taxonomy spanning Physics & Hardware, Signal Processing & ISAC Design, and Networking & Applications across near-term (1-2 yr), mid-term (3-5 yr), and long-term (5+ yr) horizons. Mode B (self-impedance sensing) is a future extension.

- [2] A. Liu, Z. Huang, M. Li, Y. Wan, W. Li, T. X. Han, C. Liu, R. Du, D. K. P. Tan, J. Lu, Y. Shen, F. Colone, and K. Chetty, "A survey on fundamental limits of integrated sensing and communication," *IEEE Commun. Surveys Tuts.*, vol. 24, no. 2, pp. 994–1034, 2022, 2nd Quart.
- [3] I. F. Akyildiz and E. P. Stuntebeck, "Wireless underground sensor networks: Research challenges," *Ad Hoc Netw.*, vol. 4, no. 6, pp. 669–686, Nov. 2006.
- [4] N. Saeed, M.-S. Alouini, and T. Y. Al-Naffouri, "Toward the Internet of underground things: A systematic survey," *IEEE Commun. Surveys Tuts.*, vol. 21, no. 4, pp. 3443–3466, 2019, 4th Quart.
- [5] I. F. Akyildiz, P. Wang, and Z. Sun, "Realizing underwater communication through magnetic induction," *IEEE Commun. Mag.*, vol. 53, no. 11, pp. 42–48, Nov. 2015.
- [6] H. Ma, E. Liu, W. Ni, Z. Fang, R. Wang, Y. Gao, D. Niyato, and E. Hossain, "Through-the-earth magnetic induction communication and networking: A comprehensive survey," *IEEE Commun. Surveys Tuts.*, vol. 28, pp. 2263–2305, 2025.
- [7] M. Cui, Z. Wu, Y. Lu, X. Wei, and L. Dai, "Near-field MIMO communications for 6G: Fundamentals, challenges, potentials, and future directions," *IEEE Commun. Mag.*, vol. 61, no. 1, pp. 40–46, Jan. 2023.
- [8] Z. Sun and I. F. Akyildiz, "Magnetic induction communications for wireless underground sensor networks," *IEEE Trans. Antennas Propag.*, vol. 58, no. 7, pp. 2426–2435, Jul. 2010.
- [9] B. Gulbahar and O. B. Akan, "A communication theoretical modeling and analysis of underwater magneto-inductive wireless channels," *IEEE Trans. Wireless Commun.*, vol. 11, no. 9, pp. 3326–3334, Sep. 2012.
- [10] S. Kisseleff, I. F. Akyildiz, and W. H. Gerstacker, "Throughput of the magnetic induction based wireless underground sensor networks: Key optimization techniques," *IEEE Transactions on Communications*, vol. 62, no. 12, pp. 4426–4439, 2014.
- [11] A. Markham and N. Trigoni, "Magneto-inductive networked rescue system (MINERS): Taking sensor networks underground," in *Proc. ACM/IEEE IPSN*, 2012, pp. 317–328.
- [12] S.-C. Lin, I. F. Akyildiz, P. Wang, and Z. Sun, "Distributed cross-layer protocol design for magnetic induction communication in wireless underground sensor networks," *IEEE Trans. Wireless Commun.*, vol. 14, no. 7, pp. 4006–4019, Jul. 2015.
- [13] M. B. Kraichman, "Impedance of a circular loop in an infinite conducting medium," *J. Res. Nat. Bureau Standards D: Radio Propag.*, vol. 66D, no. 4, pp. 499–503, 1962.
- [14] Z. Sun and I. F. Akyildiz, "Optimal deployment for magnetic induction-based wireless networks in challenged environments," *IEEE Trans. Wireless Commun.*, vol. 12, no. 3, pp. 996–1005, Mar. 2013.
- [15] Y. Li, S. Wang, C. Jin, Y. Zhang, and T. Jiang, "A survey of underwater magnetic induction communications: Fundamental issues, recent advances, and challenges," *IEEE Commun. Surveys Tuts.*, vol. 21, no. 3, pp. 2466–2487, 2019, 3rd Quart.



Haofan Dong (hd489@cam.ac.uk) is a Ph.D. student in the Internet of Everything (IoE) Group, Department of Engineering, University of Cambridge, UK. He received his MRes from CEPS CDT based in UCL in 2023. His research interests include integrated sensing and communication (ISAC), space communications, and THz communications.



Ozgur B. Akan (oba21@cam.ac.uk) received his Ph.D. degree from the School of Electrical and Computer Engineering, Georgia Institute of Technology, Atlanta, in 2004. He is currently the Head of the Internet of Everything (IoE) Group, Department of Engineering, University of Cambridge, and the Director of the Centre for NeXt-Generation Communications (CXC), Koç University. His research interests include wireless, nano-, and molecular communications, and the Internet of Everything.